Nanoscale Res Lett (2008) 3:36–44
DOI 10.1007/s11671-007-9111-3

NANO EXPRESS

Sulfonated Styrene-(ethylene-co-butylene)-styrene/ Montmorillonite Clay Nanocomposites: Synthesis, Morphology, and Properties

Anirban Ganguly · Anil K. Bhowmick

Received: 20 August 2007 / Accepted: 28 November 2007 / Published online: 18 December 2007

Abstract Sulfonated styrene-(ethylene-butylene)-styrene triblock copolymer (SSEBS) was synthesized by reaction of acetyl sulfate with SEBS. SSESB-clay nanocomposites were then prepared from hydrophilic Na-montmorillonite (MT) and organically (quaternary amine) modified hydrophobic nanoclay (OMT) at very low loading. SEBS did not show improvement in properties with MT-based nanocomposites. On sulfonation (3 and 6 weight%) of SEBS, hydrophilic MT clay-based nanocomposites exhibited better mechanical, dynamic mechanical, and thermal properties, and also controlled water–methanol mixture uptake and permeation and AC resistance. Microstructure determined by X-ray diffraction, atomic force microscopy, and transmission electron microscopy due to better dispersion of MT nanoclay particles and interaction of MT with SSEBS matrix was responsible for this effect. The resulting nanocomposites have potential as proton transfer membranes for Fuel Cell applications.

Key words SEBS · Sulfonation · Montmorillonite clay · Nanocomposites

Introduction

In recent years, there has been considerable interest in special composite materials that consist of a matrix, usually a polymer, filled with plate-like or flake-like inorganic fillers having at least one dimension in nanometer length scale and high aspect ratio. Such fillers can be extremely effective in modifying the properties of polymers. Several orders of change in mechanical, transport, rheological, electrical, or thermal properties have been demonstrated in these composites containing only a few volume percent of nano-filler [1–9].

SEBS, (styrene-ethylene-butylene-styrene) triblock copolymer, chosen as the base material in this work, is extensively used as a thermoplastic elastomer [10]. This is a nonpolar polymer and not compatible with a polar substance. Hence, polar modification of SEBS has gained recent attention. However, till now most researchers have concentrated on the maleation of SEBS with maleic anhydride in organic solution or in the melt or graft copolymerization of SEBS with methacrylic acid in organic solution. Though sulfonation of SEBS has been reported in literature [11–17], no report is available on the montmorillonite clay (MT)-based nanocomposites of sulfonated SEBS. The authors have reported earlier preparation and properties of SEBS–MT-based nanocomposites [18, 19] and numerous other rubber–clay nanocomposites from this laboratory [20–25]. A few reports on polymer composites acting as proton conducting membranes [26, 27] and a few on block copolymer–clay nanocomposites [28–33] are available. Sulfonated SEBS-montmorillonite clay-based nanocomposite as a strong member for controlling the proton transfer is a novel approach in this new field of renewable energy source in a world of crisis of energy.

This is a new approach as all the earlier studies on SEBS-MT clay nanocomposites have concentrated on intercalating the clay after organically modifying it by long-chain amines. Here, in this present work, unmodified clay (MT) has been successfully intercalated and exfoliated by sulfonated SEBS systems. The work reported here is concerned with the synthesis of sulfonated SEBS, and preparation and characteristics of the unmodified

A. Ganguly · A. K. Bhowmick (✉)
Rubber Technology Centre, Indian Institute of Technology, Kharagpur, Kharagpur 721302, India
e-mail: anilkb@rtc.iitkgp.ernet.in

montmorillonite clay (MT)-based nanocomposites. Low-cost montmorillonite clay can be used in place of organically modified nanoclays in making nanocomposites with sulfonated SEBS.

Experimental

Starting Materials

(styrene-ethylene-butylene-styrene) triblock copolymer (SEBS) with molecular weight $M_n = 50{,}000$ and styrene/ethylene-butylene (w/w) = 30/70 was supplied by Shell Chemical Co, USA. Acetic anhydride (Analytical grade) was procured from Aldrich, Milwaukee, WI. 1,2-dichloro ethane (DCE), sulfuric acid (assay content, >99%), methanol, and tetra-hydrofuran (THF, analytical grade) were obtained from Merck Ltd., Mumbai, India. Unmodified sodium montmorillonite clay (MT, having cation exchange capacity = 92.6 meq./100 gm with 2:1 tetrahedral:octahedral layer structure) and long-chain quaternary ammonium ion-modified nanoclay (OMT, *Cloisite*®20*A*) were generously supplied by Southern Clay Products, Gonzales, TX, USA. Double deionized water was prepared in this laboratory.

Sulfonation Reaction

Sulfonation was carried out onto SEBS backbone in an analogous method to that described by Weiss et al. [11] Acetyl sulfate was synthesized at temperature near to −20 °C as per Scheme 1 in dry oxygen free N_2 atmosphere.

A solution of SEBS (10% w/v in DCE) was prepared in a three necked round bottom flask equipped with condenser and the solution was heated to 60 °C and stirred for 4 h for full solubilization of SEBS. O_2 free dry N_2 gas was passed through the polymer solution in order to drive out the dissolved oxygen present in the solvent and also in the reaction flask. The required amount of freshly prepared acetyl sulfate was then added drop-wise to the reaction mixture. The reaction mixture (Scheme 2) was maintained at 60 °C under stirring in nitrogen atmosphere. After 2 h of

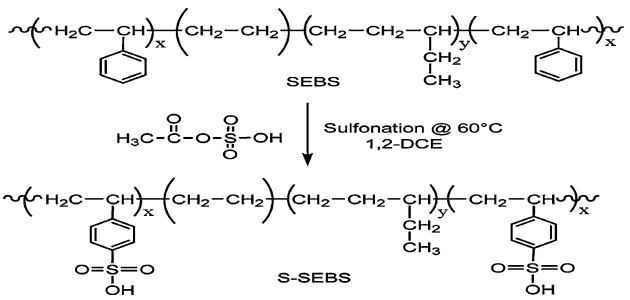

Scheme 2 Sulfonation reactions: SEBS reacts with acetyl sulfate to form SSEBS

optimized reaction time at this condition, the reaction was stopped by gradually adding an excess of isopropanol for 10 min and cooling to room temperature. Finally, the sulfonated SEBS was isolated, steam stripped in excess of double de-ionized (dd) boiling water, followed by washing several times with boiling and cold dd water (to eliminate the solvent, free acids, and hydrolyze the acetyl sulfate). The product was filtered and dried under vacuum at 70 °C up to a constant weight and was stored in a desiccator to avoid moisture.

Sulfonated SEBS (SSEBS) was dissolved in a THF/methanol mixture (9/1 v/v) and the homogeneous solution was left under stirring for 2 h after which the solvents were evaporated under reduced pressure (about 1 mmHg) at 50 °C for 7 days.

Measurement of Percentage Sulfonation

The dried sulfonated SEBS samples were weighted (W_g) and the extent of grafting was calculated from the weight gain by the samples using the following equation:

$$\% \text{ Grafting} = \left[\frac{W_g - W_0}{W_0}\right] \times 100 \quad (1)$$

where, W_0 = weight of neat SEBS and W_g = weight of the sulfonic acid-grafted SEBS. Infrared Spectroscopy (Perkin Elmer FTIR–spectrophotometer) and elemental analysis (CHNSO Analyzer, Perkin Elmer) were also performed to quantify the graft percentage. Both the results revealed ~3 and ~6 wt.% of sulfonation onto SEBS backbone.

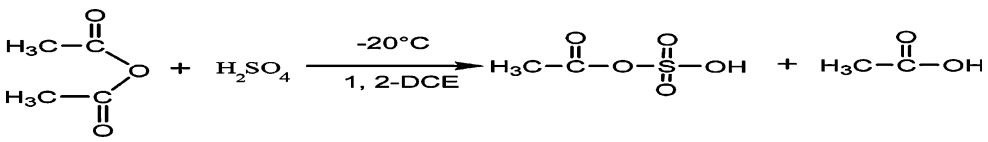

Scheme 1 Sulfonation reactions of SEBS, preparation of sulfonating agent (acetyl sulfate): acetic anhydride reacts with sulfuric acid to form acetyl sulfate and acetic acid

SSEBS Clay Hybrid Nanocomposite Film Preparation

S3SEBS (with 3 wt.% sulfonation to SEBS) and S6SEBS (with 6 wt.% sulfonation to SEBS)/ MT4 and OMT4 clay nanocomposites (with 4 wt.% of clay) were prepared using a THF solvent-casting method. Initially, SSEBS was dissolved in THF overnight and MT or OMT clay at optimized 4 wt.% were suspended in THF for 6 h and stirred for 2 h using a magnetic stirrer. The polymer solution and clay particle suspension were then mixed together at 25 °C and stirred for 1 day in order to complete the mixing. Next, the samples were dried in a hood by evaporating the solvent to get a film thick in the range of 50–60 μm.

Fourier Transform Infrared (FT-IR) Spectroscopic Studies

*FT-IR*studies were carried out in dispersive mode on thin film samples using Perkin Elmer FTIR–spectrophotometer (model Spectrum RXI,UK), within a range of 400–4,400 cm^{-1} using a resolution of 4 cm^{-1}. An average of 32 scans have been reported for each sample.

Microstructure by Wide Angle X-ray Diffraction (WAXD)

Wide angle X-ray diffraction analysis of the nanocomposites was carried out in a *PANalytical XPert Pro (3040/60 the Netherlands)* X-ray diffractometer (operated at 30 kV and 40 mA) at room temperature, equipped with Cu–K_a radiation.

The scanning rate was 1°/min and the range of Goniometer angle (2θ) was from 2°–10°. Subsequently, the d-spacing of the clay layers was calculated using the Bragg's equation,

$$n\lambda = 2d\,\mathrm{Sin}\theta \quad (2)$$

where λ = wavelength of the X-ray with Cu–K_a target = 0.154 nm, d = interplanar distance of the clay platelets, θ = angle of the incident radiation.

Morphological Investigation

Transmission Electron Microscopy (TEM)

The samples for transmission electron microscopy analysis were prepared by ultra cryo-microtomy using a *Leica Ultracut UCT (Wien, Austria)*. Freshly sharpened glass knives with cutting edge of 45° were used to get the cryosections of 50–70 nm thickness at a sub-ambient temperature of −80 °C using a *JEOL 2010, Japan* TEM, operating at an accelerating voltage of 200 kV. Selective staining of aromatic moieties in the samples was done with vapor of OsO_4.

Phase Imaging by Atomic Force Microscopy (AFM)

The effects of sulfonation on SEBS and of inclusion of inorganic silicate clay layers on the morphology of SEBS and its nanocomposite were investigated by using atomic force microscopy (*MultiMode AFM*^{TM} from Digital Instruments, Santa Barbara, CA, USA) in air at ambient conditions (25 °C, 60% RH) in the tapping mode using etched silicon probe tips (TESP), with a spring constant in the range of 40 N/m. For each sample, minimum three images were analyzed.

Dynamic Mechanical Thermal Analysis (DMTA)

The dynamic mechanical spectra of the samples were obtained by using *Rheometric Scientific DMTA IV, NJ, USA* analyzed in tension-compression mode at a constant frequency of 1 Hz, a strain of 0.01%, and a temperature range from −100 to 130 °C at a heating rate of 2 °C/min. The temperature corresponding to the peak in tanδ versus temperature plot was taken as the glass–rubber transition temperature (T_g).

Studies of Mechanical Properties

Tensile properties were measured on dumb-bell specimens at room temperature using a ZWICK Z010 tensile test machine (Zwick Inc., Ulm, Germany). The gauge length and cross-head speed were 25 mm and 500 mm/min, respectively. At least five samples were tested and the average was used.

Thermogravimetric Analysis (TGA)

The thermal degradation analysis of SEBS, grafted SEBS, and their nanocomposites was performed with *TGA Q50* of TA Instruments- Waters LLC, USA operated at a heating rate of 20 °C/min in N_2 atmosphere at a flow rate of 60 mL/min in the temperature range of 25–700 °C.

Water–Methanol Uptake and Permeability

The films of sulfonated SEBS and their MT-based nanocomposites were soaked in deionized water–Methanol (80–20) mix for 3 weeks to determine the uptake content by the following Eq. 3:

$$\text{Uptake content} = \frac{(w_{\text{wet}} - w_{\text{dry}})}{w_{\text{dry}}} \times 100 \quad (3)$$

where w_{wet} = weight of wet samples after blotting the surface water–MeOH and w_{dry} = weight of dry sample before wetting. Permeability of water–MeOH (80–20) mix into free air through the films of SSEBS and MT4-based nanocomposites was measured by diffusion process with an airtight glass diffusion cell.

AC Resistance and Proton Conductivity

AC electrical resistance was measured at room temperature for film samples in the transverse direction with a two probe INSTEK LCR meter (LCR 819, Taiwan) operating in AC frequency range from 0.4 to 10 kHz. The proton conductivity was measured in an indirect process for the water–methanol-immersed samples after wiping out the surface water and measuring the resistance employing the same set up.

Results and Discussion

Sulfonation of SEBS

Scheme 2 portrays the synthetic route to graft $-SO_3H$ ions onto SEBS backbone. Elemental analysis by CHNSO analyzer reveals 3 and 6 wt.% of sulfonation in the SEBS backbone. FTIR spectra, shown in Fig. 1, illustrate the effect of sulfonation onto SEBS and subsequent interaction with MT clays in the nanocomposite. The characteristics peak for SEBS at 1,602 cm^{-1} for aromatic system stays is observed for all the samples. The peaks at 2,850, 2,920, and 1,465 cm^{-1} for stretching of $–CH_3$ and $–CH_2$ remain in their respective position and their intensity indicates that no sulfonation has taken place in mid ethylene–butylene block of SEBS. The peak at 699 $cm^{-1}$for styrenic moiety of SEBS has shown change in the intensity mostly due to sulfonation. The band near 1,125–1,160 cm^{-1} and the peaks at 1,376, 1,010, and 1,035 cm^{-1} are all due to grafted sulfonic acid group in the samples. The peak at 756 cm^{-1} appears due to mono-substituted benzene ring which is clear from the reaction scheme shown in Scheme 2. Now, the spectrum for SSEBS-MT4 nanocomposite reveals that non-H- bonded OH stretching peak for MT clay at 3,634 cm^{-1} and –OH bending peak at 1,641 cm^{-1} vanish in the resulting nanocomposite due to ionic interaction of –OH group of MT clay with $–SO_3H$ group of SSEBS, as shown in Fig. 1. Asymmetric Si–O–Si stretching peak at 1,040 cm^{-1} for MT clay shifts to 1,044 cm^{-1} owing to interaction between MT clay structure and pendant sulfonated polystyrene group (shown in Scheme 2) in sulfonated SEBS . The peaks for H bonded –OH band near 3,430 cm^{-1} and the peaks at 523 and 466 cm^{-1} for MT clay shift to a little extent in the nanocomposite which retains all the peaks for sulfonate group in its spectrum.

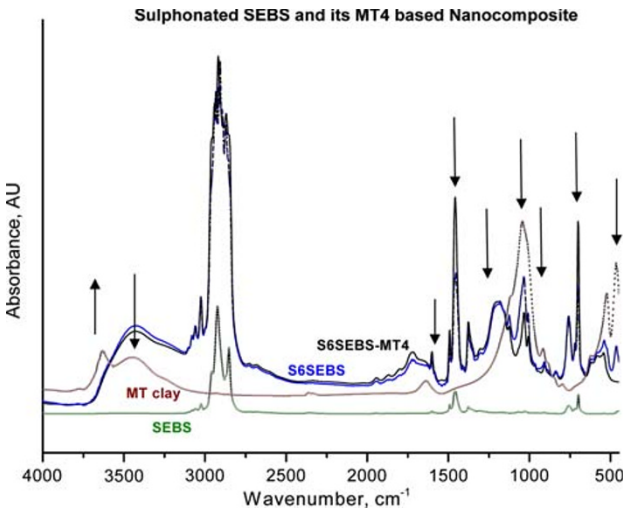

Fig. 1 FTIR traces of SSEBS, SSEBS-MT4 nanocomposite along with pristine MT clay and SEBS film

Morphological Shift on Sulfonation

Shift of surface morphology from lamellar type for neat SEBS (Fig. 2a) to slightly distorted one for S3SEBS even with very low sulfonation levels (3 wt.%) (Fig. 2b) and finally to distorted one in S6SEBS (Fig. 2c) is revealed from AFM phase images. The sulfonation brings about a disturbance in micro-phase separation in SSEBS. The sulfonated PS (SPS) domains are seen to increase in size in the resulting S6SEBS (Fig. 2c). Bright field-stained TEM images also corroborate the same findings of distorted morphology for sulfonated SEBS (Fig. 2e) from its original lamellar morphology (Fig. 2d) for neat SEBS. In the image of S6SEBS, small black distorted spherical clusters ($\sim$20 nm) corresponding to SPS domains in the matrix are obtained. This morphological shift may be the result of an increase in the Flory–Huggins interaction parameter between the two blocks, a change in the volume fraction, and/or a loss of chain mobility resulting from hydrogen-bonding after grafting. The viscoelastic study also reveals that the T_g for PS block have been shifted on sulfonation (discussed later).

Microstructure of SSEBS–Clay Nanocomposites by WAXD

In this present investigation, hydrophilic $–SO_3H$ moiety has been grafted to the PS block of SEBS as characterized

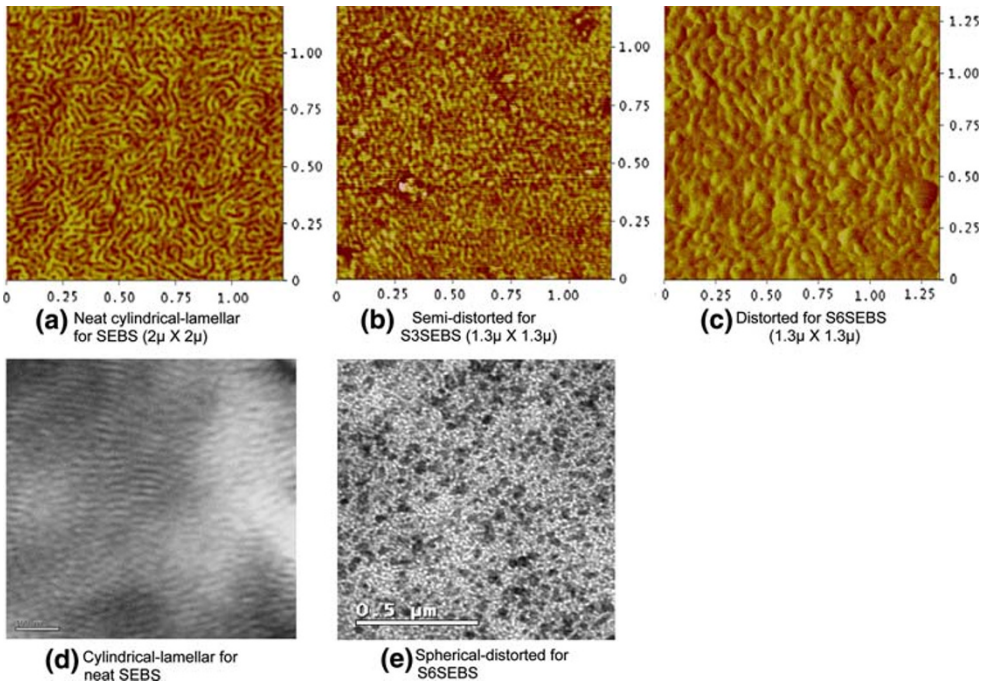

Fig. 2 Comparative surface morphologies by AFM (**a**–**c**) and bulk morphologies by bright field TEM (**d**–**e**)—before and after sulfonation of SEBS

by FTIR and morphological investigations. Onto sulfonated SEBS matrices, four parts of MT clay (MT4) have been impregnated and their microstructure has been elucidated by WAXD, TEM, AFM, and DMTA. The peak shift of MT clays corresponding to its 001 diffraction face (at 7.5°, 1.17 nm, Fig. 3) has been monitored for the nanocomposite films. This study shows that the basal spacing value for MT platelets in SEBS-MT4 stays only at 1.37 nm, indicating a small intercalation by fully hydrophobic SEBS chains. Introduction of polarity into SEBS matrix dramatically changes the microstructure of the nanocomposite prepared with the same MT clays at 4 phr of loading. The characteristic peak from MT plate in WAXD has been fully diminished in the case of S3SEBSMT4 and S6SEBSMT4 nanocomposites (Fig. 3) due to de-lamination of individual clay platelets in the entire matrix of sulfonated SEBS which has a 'polarity match' with the clay surface as a result of favorable interaction. On the contrary, the peak height of the SSEBS-OMT4 nanocomposite has gone down due to presence of lower frequency (number) of stacked clay layers and the peak position stays still at 6.3° corresponding to a basal spacing of only 1.40 nm, indicating that sulfonate group might have taken out the long-chain surfactant from the spacings of clay platelets. These results are in line with the morphological studies by AFM and TEM in the next section.

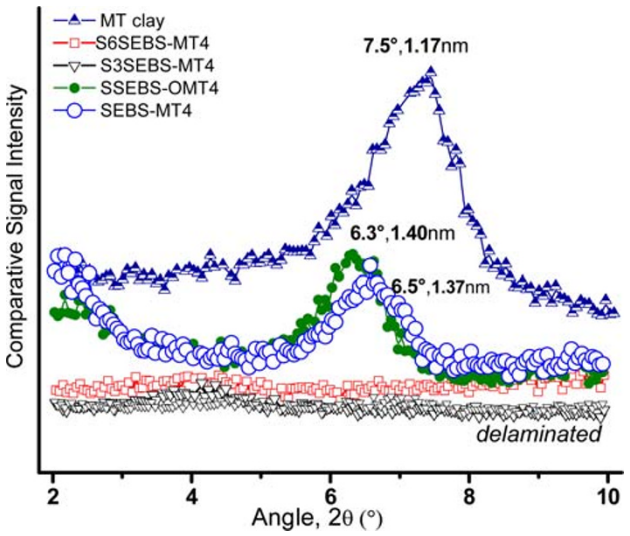

Fig. 3 X-ray diffraction pattern of MT clay, SEBSMT4, SSEBSMT4, and SSEBSOMT4 exfoliated-intercalated nanocomposites

Microstructure of Nanocomposite by TEM, AFM, and DMTA

On incorporation of MT clay in pristine SEBS matrix, only thick stacks are formed mostly due to incompatibility of hydrophobic polymer with hydrophilic MT clay particles (Fig. 4a). After grafting sulfonate groups onto SEBS, well distribution of intercalated MT clay platelets in S3SEBS matrix and exfoliated platelets in S6SEBS matrix is observed in bright field TEM images (Fig. 4b, c). It is unique to have such wonderful exfoliation of individual clay layers with the same MT clay at the same loading of 4wt% in sulfonated SEBS matrices. On the other hand, organically modified clay, OMT does not get exfoliated (10–15 nm stacks in Fig. 4d) in the same S6SEBS matrix,

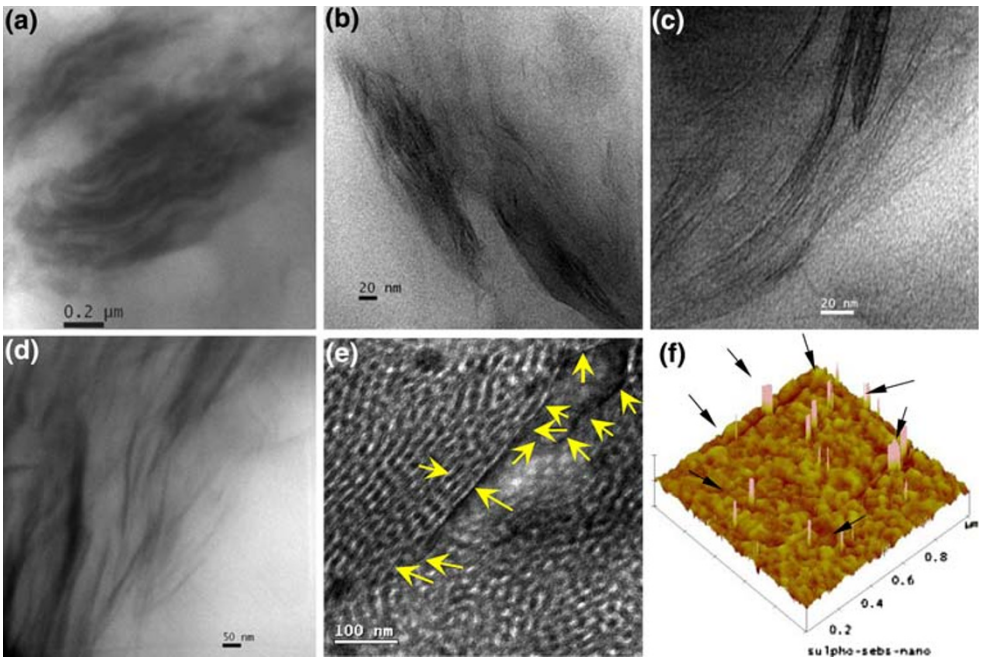

Fig. 4 Bright field TEM morphology of (**a**) thick stacks of SEBS-MT4, (**b**) intercalated-exfoliated S3SEBS-MT4, (**c**)exfoliated S6SEBS-MT4, (**d**) intercalated S6SEBS-OMT4, (**e**) regenerated distinct lamellae of SPS and PEB domains of exfoliated S6SEBS-MT4 (clays are in arrow mark positions) nanocomposites as seen after selective staining, (**f**) 3-dimensional AFM phase image of S6SEBS-MT4 showing fine clay layers (with arrow marks: 2–6-nm thick) impregnated from SPS domains of the matrix

indicating less compatibility. This is in line with the results obtained with WAXD results. Regeneration of distinct lamellae of SPS and PEB segments of exfoliated S6SEBS-MT4 (clays are in arrow mark positions) nanocomposites can be as seen (Fig. 4e) after selective staining. Fine clay layers (2–6 nm thick) have impregnated in SPS domains as shown in tapping mode AFM 3-dimensional phase image (Fig. 4f) of S6SEBS-MT4 nanocomposite. This morphology is supported well by WAXD studies and is reflected in better physico-mechanical and thermal characterization of these nanocomposites reported later. This microstructure is supported well by the viscoelastic tan delta trace for SEBS, S3SEBS, S6SEBS and S6SEBS-MT4 nanocomposite by DMTA analysis (Fig. 5). The tanδ for hard PS phase of neat SEBS shifts from 65.8 to 69.0 °C for S6SEBS without changing the position and height of rubbery phase tanδ, indicating that sulfonation has clear effect on PS domains of SEBS microstructure. Micro-phase separated morphology is thus disturbed to a greater extent in this S6SEBS, as supported by TEM and AFM studies too. Now, S6EBS-MT4 nanocomposite shows lowering of tanδ peak height (0.26 from 0.34) associated with peak broadening and +14 °C shift of SPS domains, clearly elucidating strong interaction of MT silicate layers with S6SEBS matrix in the hybrid nanocomposite.

Stress–strain Properties of Resulting SSEBS and their MT4-Based Nanocomposites

High-strain mechanical properties of neat SEBS, sulfonated SEBSS, and their MT clay-based nanocomposites are

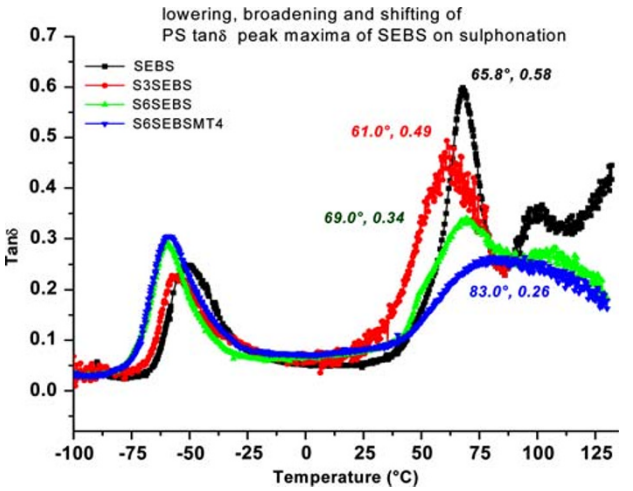

Fig. 5 Comparative tanδ traces for SEBS, S3SEBS, S6SEBS, and S6SEBS-MT4 nanocomposite

reported in Table 1. Due to almost no exfoliation of MT clays by SEBS, negligible improvement in physical properties is obtained for SEBS-MT4 system, while OMT clay exhibits much improved properties. On sulfontaion, physical properties drop down from neat SEBS due to distorted morphology. However, for the MT4 nanocomposite, much improved mechanical properties are achieved (27% & 41% improvement in tensile strength and 21% & 39% improvement in modulus) for S3SEBSMT4 and S6SEBSMT4 nanocomposites, respectively.

Proper dispersion of fine reinforcing MT clay platelets is responsible for this enhanced physical property as compared to sulfonated SEBSs.

Table 1 Tensile stress–strain of sulfonated SEBS-nanocomposites

Sample	Tensile strength (MPa)	Modulus at 50% strain (MPa)	Breaking elongation (%)
SEBS	23.6 ± 0.5	2.6 ± 0.2	520 ± 10
SEBS-MT4	24.2 ± 0.5	2.2 ± 0.1	530 ± 15
SEBS-OMT4	31.6 ± 0.7	3.5 ± 0.3	580 ± 20
S3-SEBS	20.5 ± 0.3	2.4 ± 0.2	500 ± 10
S3-SEBS-MT4	26.1 ± 0.5	2.9 ± 0.2	500 ± 10
S6-SEBS	20.0 ± 0.3	2.3 ± 0.1	460 ± 10
S6-SEBS-MT4	28.3 ± 0.6	3.2 ± 0.2	480 ± 8

Thermal Degradation Properties

Remarkable enhancement in thermal properties is observed on sulfonation of 3 and 6 wt.% onto pristine SEBS as shown by thermogravimetry (TG) and differential thermogravimetric (DTG) analysis in Fig. 6. Maximum degradation temperature has progressively increased from 415 °C for pristine SEBS to 437 °C for S3SEBS, and finally to 440 °C for S6SEBS (Fig. 6). More sulfonation has imparted more thermal stability to the systems. Initial weight loss is due to sulfonic acid groups. On synthesizing S6SEBS-MT4 nanocomposite, even further improvement in thermal stability is realized (TG maximum shifts toward 443 °C). Corresponding DTG maxima displays that the height reduces as compared to neat SEBS for S3SEBS, S6SEBS, and S6SEBS-MT4 progressively. This reduction in peak height indicates reduction in rate of degradation with the grafted species. Thus, physically stronger S6SEBS-MT4 nanocomposite shows enhanced thermal properties too.

Water–Methanol Uptake Properties

For the unique lamellar-cylindrical morphological structure and completely hydrophobic in chemical nature, it is very difficult for water or proton molecules to permeate across the SEBS neat films. As progressive sulfonation has been carried out on SEBS, hydrophilicity has been generated on the system with generation of distorted morphology. In order to investigate this quantitatively, water–methanol (80–20) uptake and permeation measurements have been carried out for neat and sulfonated SEBS systems along with their nanocomposite films. Permeation of water–MeOH through nanocomposite films reveals much improved barrier to the solvent mixture owing to torturous path provided by the finely dispersed clay platelets in the entire matrices (Fig. 7). Though neat SEBS film has not allowed water–MeOH to pass through it by diffusion mechanism, S3SEBS and S6SEBs show much water diffusion (1,445 cm^3/7day and 2,445 cm^3/7day) as depicted in Fig. 7. Around 21% and 91% improvements have been imposed by S3SEBSMT4 and S6SEBSMT4 nanocomposites, respectively for permeation of water–MeOH. It gives a clear picture of benefit of corresponding MT4-based nanocomposites with respect to S3SEBs or S6SEBS. On immersing the films in water–MeOH mixture, controlled water–MeOH uptake (181% less uptake for S6SEBSMT4 from S6SEBS and 76% less for S3SEBSMT4 from S3SEBS) is evident from Fig. 8. The controlled water uptake and diffusion are achieved even in interconnected and frustrated morphology of sulfonated SEBS (as elucidated from AFM and TEM images and DMTA) due to proper dispersion of MT nanoclays in the resulting nanocomposites.

AC Resistance in Dry and Wet Modes

This tremendous improvement in water–MeOH uptake and permeation picks up these nanocomposites as interesting

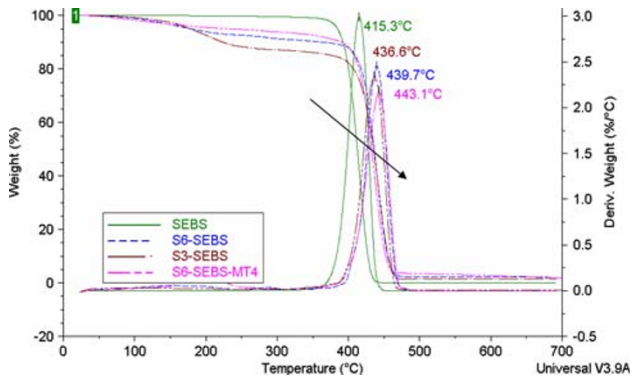

Fig. 6 Extraordinary improvement in thermal stability of SEBS as revealed from TGA and DTG curves for SEBS, S3-SEBS, S6-SEBS, and S6-SEBS-MT4

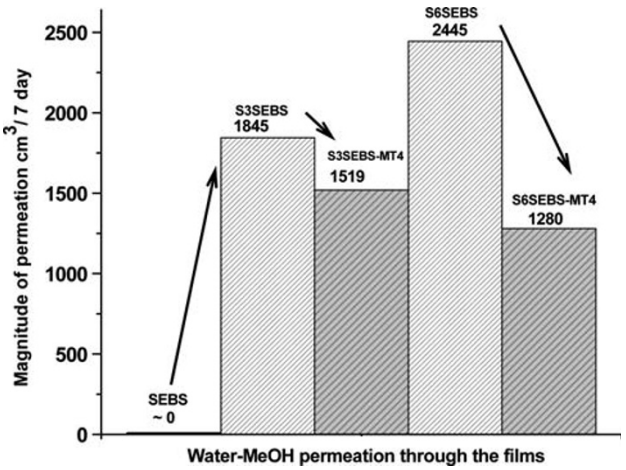

Fig. 7 Permeation of water–MeOH through sulfonated SEBS and MT4-based nanocomposite films

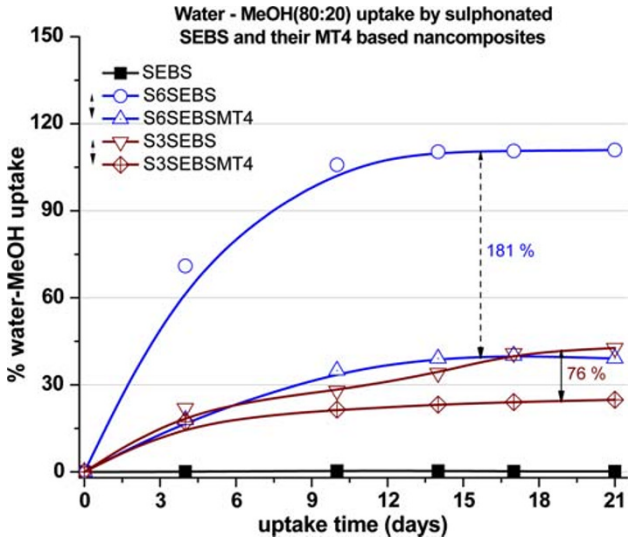

Fig. 8 Tremendous improvement in controlled water–methanol (80:20) uptake by sulfonated SEBS and their MT4 nanocomposites

members for membranes to be used as Direct Methanol Fuel Cell (DMFC). Although sulfonated SEBS has been studied as new polymeric materials for DMFC [34–37], no specific report directs their montmorillonite clay-based nanocomposites in the same application. The present investigation gives an insight to controlled AC resistance and proton conductivity of these nanocomposite films from their base matrices. From Fig. 9, it is clear that SEBS does not conduct electricity at a frequency range of 0.4–3 kHz, while S3SEBS and S6SEBS show progressive improvement in conduction. SSEBS-MT4 nanocomposites control this flow of electron or ion. After immersing the same samples in water–MeOH mixture for 7 days, resistance for all the samples has tendency to go down with nanocomposite, again playing a role of control for methanol crossover. In the protonated solvent wet samples, the hydrophilic ion channels which are helpful to the movement of protons in sulfonated SEBS system, the AC resistance becomes less compared to the dry samples.

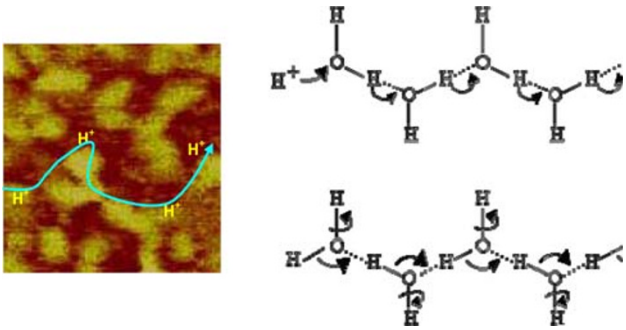

Scheme 3 Preferential route and mechanism of proton transfer through the edges of SPS domains in water-wet condition of SSEBS

Proton conductivity and dimensional stability of the films are closely related to their morphology.

Scheme 3 shows the possible route of protons through the sulfonated PS domains and preferential affinity in the SSEBS matrix. As water is a good conductor of protons, the H^+ conduction occurs through "hop-turn" mechanism as shown in this scheme due to H-bonded network between protonated water molecules. When MT clays are there in the nanocomposite, these H^+ interact with the acid group as well as with –OH group of clay, thereby control the transfer of protons through the films.

Conclusions

1. SEBS has been sulfonated at two different levels of sulfonation (3 and 6 wt.%) by in situ-prepared acetyl sulfate. FTIR spectra and DMTA analysis confirm that grafting has taken place at the end PS blocks of SEBS.
2. On sulfonation, micro-phase-separated morphology has been shifted from purely cylindrical for neat SEBS to distorted-spherical mixed one for S3SEBS and distorted one for S6SEBS.
3. Unmodified montmorillonite clay (MT)-based nanocomposites have been synthesized based on these

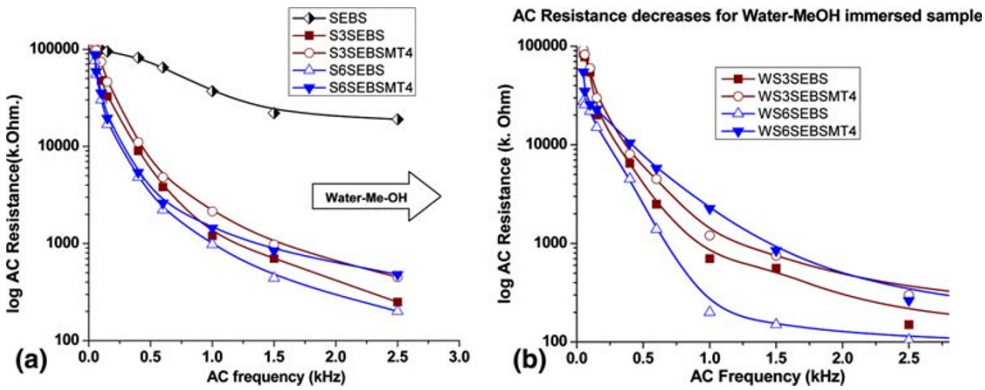

Fig. 9 Lowering in AC electrical resistance properties of (**a**) S3SEBS, S6SEBS, and S6SEBS-MT4 films on (**b**) immersion in water–MeOH (80:20) mixture for 7 days

sulfonated SEBS following solution intercalation process.

4. The dispersion of MT clays in neat SEBS matrix was a real problem as evidenced from morphology and reflected in its properties. Hydrophilic MT clays have been better dispersed and intercalated in these SSEBS matrices and MT clay-based nanocomposites exhibit enhanced mechanical and thermal properties as compared SEBS-MT and SEBS-OMT. XRD and TEM studies reveal better interaction and dispersion of MT with SSEBS matrix. Remarkable improvement in thermal degradation resistance for S6SEBS-MT4 is observed.
5. Water–MeOH uptake and permeation is much improved for corresponding nanocomposites making them potential candidate for DMFC.
6. AC resistance is shown to decrease on water–MeOH wet samples with nanocomposites posing restrictions for electricity flow owing to the torturous path in the matrix.
7. From this study, it is proved that organic modification of clay is not mandatory in making polymer–clay nanocomposites. Polar modification of the SEBS matrix by sulfonation enables cheaper MT clays to be used to synthesize excellent nanocomposites with enhanced physico-mechanical, thermal, water swelling, and electrical properties.

Acknowledgments Anirban Ganguly acknowledges the scholarship grant in NDF category by AICTE, New Delhi, India.

References

1. A. Usuki, Y. Kojima, M. Kawasumi, A. Okada, Y. Fukushima, T. Kurauchi, O. Kamigaito, J. Mater. Res. **8**, 1174 (1993)
2. T.J. Pinnavaia, G.W. Beall (eds.), *Polymer–Clay Nanocomposites* (John Wiley & Sons, Inc., New York, 2000)
3. E.P. Giannelis, R. Krishnamoorti, E. Manias, Adv. Polym. Sci. **138**, 108 (1999)
4. R. Krishnamoorti, R.A. Vaia, in *Polymer Nanocomposites: Synthesis, Characterization, and Modeling* (ACS Symposium Series 804, Washington DC, 2001)
5. R.A. Vaia, E.P. Giannelis, Macromolecules **30**, 8000 (1998)
6. A.B. Morgan, J.W. Gilman, J. Appl. Polym. Sci. **87**, 1329 (2003)
7. S.S. Roy, M. Okamoto, Prog. Polym. Sci. **28**, 1539 (2003)
8. Y.H. Hyun, S.T. Lim, H.J. Choi, M.S. Jhon, Macromolecules **34**, 8084 (2001)
9. J.W. Kim, S.G. Kim, H.J. Choi, M.S. Jhon, Macromol. Rapid Comm. **20**, 450 (1999)
10. N.R. Legge, G. Holden, H.E. Schroeder (eds.), *Thermoplastic Elastomers: A Comprehensive Review* (Oxford University Press, New York, 1987)
11. R.A. Weiss, A. Sen, C.A. Willis, L.A. Pottick, Polymer **32**, 1867 (1991)
12. X. Lu, W.P. Steckel, R.A. Weiss, Macromolecules **26**, 5876 (1993)
13. R.F. Storey, D.W. Baugh, Polymer **41**, 3205 (2000)
14. A. Mokrini, J.L. Acosta, Polymer **42**, 9 (2001)
15. K.A. Mauritz, R.F. Storey, D.A. Mountz, D.A. Reuschle, Polymer **43**, 4315 (2002)
16. R.I. Blackwell, K.A. Mauritz, Am. Chem. Soc. Polym. Prepr. **43**, 1341 (2002)
17. K.A. Mauritz, R.F. Storey, D.A. Reuschle, N.B. Tan, Polymer **43**, 5949 (2002)
18. A. Ganguly, M. DeSarkar, A.K. Bhowmick, J. Appl. Polym. Sci. **100**, 2040 (2006)
19. A. Ganguly, M. DeSarkar A.K. Bhowmick, J. Polym. Sci.: Part B Polym. Phys. **45**, 52 (2007)
20. S. Ray, A.K. Bhowmick, Rubber Chem. Technol. **74**, 835 (2001)
21. M. Pramanik, S.K. Srivastava, B.K. Samantaray, A.K. Bhowmick, J. Polym. Sci. Part B: Polym. Phys. **40**, 2065 (2002)
22. S. Sadhu, A.K. Bhowmick, Rubber Chem. Technol. **76**, 0860 (2003)
23. S. Sadhu, A.K. Bhowmick, J. Polym. Sci.: Part B: Polym. Phys. **42**, 1573 (2004)
24. M. Maiti, A.K. Bhowmick, J. Polym. Sci.: Part B Polym. Phys. **44**, 162 (2006)
25. A.K. Bhowmick, A. Ganguly, M. Maiti, Kautsc. Gumm. Kunstst. **59**, 437 (2006)
26. P.P. Kundu, V. Sharma, Y.G. Shul, Critic. Rev. Solid Stat. Mat. Sci. **32**, 51 (2007)
27. Sangeetha D., Int. J. Polym. Mat. **56**, 535 (2007) and references therein
28. J. Ren, A.S. Silva, R. Krishnamoorti, Macromolecules **33**, 3739 (2000)
29. R. Krishnamoorti, A.S. Silva, C.A. Mitchell, J. Chem. Phys. **115**, 7175 (2001)
30. A.S. Silva, C.A. Mitchell, M.F. Tse, H.C. Wang, R. Krishnamoorti, J. Chem. Phys. **115**, 7166 (2001)
31. H. Hasimoto, M. Fujimura, T. Hashimoto, H. Kawai, Macromolecules **14**, 844 (1981)
32. S.T. Lim, C.H. Lee, Y.K. Kwon, H.J. Choi, J. Macromol. Sci. Part B: Phys. **43**, 577 (2004)
33. C.H. Lee, H.B. Kim, S.T. Lim, H.S. Kim, Y.K. Kwon, H.J. Choi, Macromol. Chem. Phys. **207**, 444 (2006)
34. S.G. Ehrenberg, J.M. Serpico, G.E. Wnek, J.N. Rider, U.S. Patent. 5468574, 13 (1997)
35. S. Butkewitsch, J. Scheinbeim, Appl. Surf. Sci. **252**, 8277 (2006)
36. C.A. Edmondson, J.J. Fontanella, S.H. Chung, S.G. Greenbaum, G.E. Wnek, Electrochim. Acta. **46**, 1623 (2001)
37. B. Kim, J. Kim, B.J. Cha, B. Jung, J. Memb. Sci. **280** 270 (2006)